

Supplementary Information for

Controlled Growth of a Line Defect in Graphene and implications for Gate-Tunable Valley Filtering

J.-H. Chen^{1,2,¶}, G. Autès³, N. Alem^{1,2,δ}, F. Gargiulo³, A. Gautam⁴, M. Linck^{4,5},
C. Kisielowski⁴, O. V. Yazyev³, S. G. Louie^{1,2} and A. Zettl^{1,2}

¹Department of Physics, University of California at Berkeley, Berkeley, CA 94720, USA

²Materials Science Division, Lawrence Berkeley National Laboratory, Berkeley, CA 94720, USA

³Institute of Theoretical Physics, Ecole Polytechnique Fédérale de Lausanne (EPFL), CH-1015 Lausanne, Switzerland

⁴National Center for Electron Microscopy, Lawrence Berkeley National Laboratory, Berkeley, CA 94720, USA

⁵CEOS-GmbH, Englerstr. 28, D-69126 Heidelberg, Germany

*Correspondence to: azettl@berkeley.edu

[¶]Current Address: International Center for Quantum Materials, School of Physics, Peking University, Beijing, China 100871

^δCurrent Address: Department of Materials Science and Engineering, Pennsylvania State University, University Park, PA 16802, USA

[†]Current Address: CEOS-GmbH, Englerstr. 28, D-69126 Heidelberg, Germany

1. Temperature Estimations

The temperature of graphene under large current bias during the experiment was estimated from finite-element simulation using Ansys Workbench. Graphene/Silicon Nitride bilayer of $500 \mu\text{m} \times 500 \mu\text{m}$ was used in the model. The detail parameters are: the thermal

conductivity of graphene $\kappa_{\text{Graphene}} = \frac{5000}{1 + 0.01(T - 350K)} \text{ Wm}^{-1}\text{K}^{-1}$ and silicon nitride thin film

$\kappa_{\text{SiliconNitride}} = 3.365 \text{ Wm}^{-1}\text{K}^{-1}$ (the mean value from Refs. ² and ³); the electrical resistivity of the

CVD graphene film is measured to be $\rho_{\text{Graphene}} = 2.5 \text{ k}\Omega/\square$ and current

density $j_{\text{Graphene}} \approx 1.5 \times 10^{10} \text{ A/m}^2$, assuming a thickness of graphene to be 0.36 nm; the thermal

resistivity at the graphene-silicon nitride interface $r_{G-S} = 4.2 \times 10^{-8} \text{ Km}^2\text{W}^{-1}$ [1], and the emissivity of graphene $\varepsilon_{\text{Graphene}} = 0.023$ [1, 4] and silicon nitride $\varepsilon_{\text{SiliconNitride}} = 0.2$ [5]. The boundary conditions are: the temperature at the boundary of $500 \mu\text{m} \times 500 \mu\text{m}$ square was set to be 298K, while graphene and silicon nitride radiates into an environment of 298K, convection is set to be zero since the sample was under high vacuum during the experiment. The model geometry and the temperature distribution are shown in Figures S1a and S1b. Note that the thickness of the graphene/silicon nitride bilayer is not to scale. All the data was collected in the central region where the temperature of the graphene sample is about 1300K. Using the resistivity and current density data from above, the total power input to the system is calculated as 18.225 mW. The total heat flux out of the four edges of the graphene-silicon nitride bilayer can be estimated from the simulation to be about 13 mW, indicating that about 5 mW was dissipated through radiation.

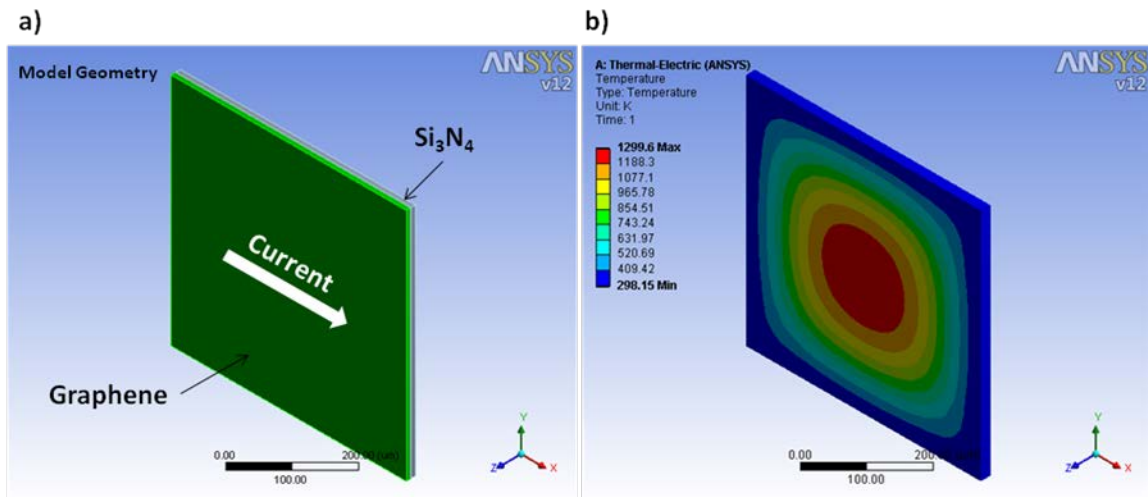


Figure S1. Finite element simulation of the temperature of graphene sample during the electrical biasing experiment. a) The graphene/silicon nitride bilayer model; b) simulated temperature distribution of the graphene device during experimental conditions.

2. Instrumentation and imaging conditions

The TEAM 0.5 microscope, which is equipped with Cs corrector, was used in this study. All the images in this publication were taken at 80 kV. To enable atomic resolution at the low accelerating voltage, the resolution-limiting effect of chromatic aberration was reduced by using a monochromator to limit the energy width in the illuminating electron beam. For imaging, a focal

series of images were recorded by TEAM 0.5 microscope and the electron exit wave was reconstructed using the MacTempas image processing and simulation software. The phase of the electron exit wave was reconstructed⁶ from the focal series using the following parameters:

Third and fifth order spherical aberration: $C_3 = -6 \mu\text{m}$, $C_5 = 4.5 \text{ mm}$,

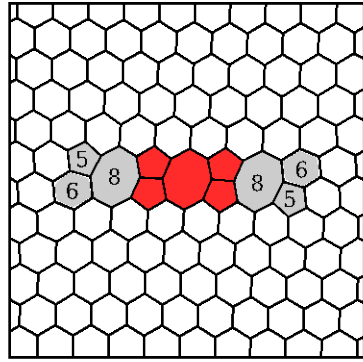
Focus step size = 10 \AA .

To further correct for the residual lens aberrations, two fold astigmatism of 120 \AA in the direction of 134 degrees, and three fold astigmatism of 700 \AA in the direction of 0 degree were introduced into the propagated wave. In addition, coma was set to 183 \AA in the direction of 50 degrees.

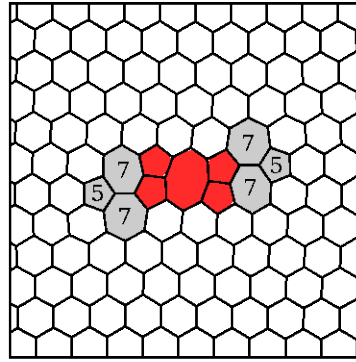
3. Calculation of the formation energies of 7-7-5 and 5-6 termination structures

In order to investigate the formation energies of different defect terminations, we performed calculations on the finite segments of line defect of varying length. Due to the long-ranged strain fields produced by the studied defects, sufficiently large models have to be considered. In particular, in our simulations the defects were embedded in a rectangular periodic supercell of graphene containing 1200 atoms. Models of this size are difficult to treat using first-principles techniques, thus the present simulations have been performed using the classical force field approach implemented in the LAMMPS package⁷. We used the AIREBO potential.

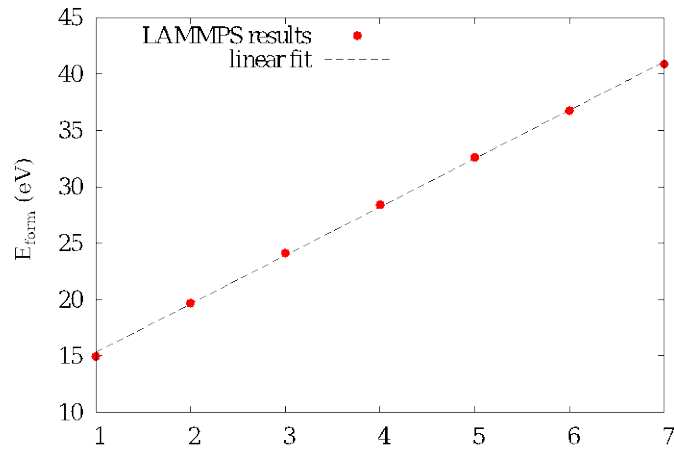
Two structural models of short line defects with 5-6 and 7-7-5 terminations characterized by formation energies of 18.13 eV and 14.97 eV, respectively, are shown in Figs. S2a and S2b. We found that equal-length line defects with 7-7-5 terminations are generally more stable than the 5-6-terminated line defects by $\sim 3 \text{ eV}$ (i.e. by $\sim 1.5 \text{ eV}$ per termination). Figure S2c shows the dependence of the formation energy of 7-7-5-terminated line defect on its length expressed in terms of the number of 5-5-8 structural units. While the smallest defect considered has formation energy of 14.97 eV, its elongation by each additional 5-5-8 unit increases the formation energy by 4.42 eV.



a) 5-6 termination - $E_{\text{form}}=18.13\text{eV}$



b) 7-7-5 termination - $E_{\text{form}}=14.97\text{eV}$



c) Length of the line defect (number of 5-5-8 cells)

Figure S2. Atomic structures of short (a) 5-6- and (b) 7-7-5-terminated line defects. (c) Formation energy of a 7-7-5-terminated line defect as a function of its length expressed in terms of the number of 5-5-8 structural units.

References

- ¹ M. Freitag, M. Steiner, Y. Martin, V. Perebeinos, Z. Chen, J. C. Tsang, and P. Avouris, *Nano Lett.* 9, 1883 (2009).
- ² P. Eriksson, J. Y. Andersson, and G. Stemme, *J. Microelectromechanical Syst.* 6, 55 (1997).
- ³ M. von Arx, O. Paul, and H. Baltes, *J. Microelectromechanical Syst.* 9, 136 (2000).
- ⁴ R. R. Nair, P. Blake, A. N. Grigorenko, K. S. Novoselov, T. J. Booth, T. Stauber, N. M. R. Peres, and A. K. Geim, *Science* 320, 1308 (2008).
- ⁵ F. Völklein, *Thin Solid Films* 188, 27 (1990).
- ⁶ A. Thust, W. M. J. Coene, M. Op de Beeck, and D. Van Dyck, *Ultramicroscopy* 64, 211 (1996).
- ⁷ S. Plimpton, *J. Comp. Phys.* 117, 1 (1995).